Jestr

Journal of Engineering Science and Technology Review 15 (5) (2022) 145 - 152

Research Article

JOURNAL OF
Engineering Science and Technology Review

www.jestr.org

Indirect Matrix Converter Controlled with ANFIS-based Modulation

Murikipudi Nagaraju[1,*], G. Durga Sukumar[1] and M. Ravindrababu[2]

[1]*Vignan Institute of Technology and Science, Deshmuki, Yadadri, Bhuvanagiri, Telengana, 508284, India*
[2]*University College of Engineering Narsasraopet, JNTUK, Guntur, A.P., 522601, India*

Received 19 July 2022; Accepted 15 November 2022

Abstract

A matrix converter is a one level converter; it converts from AC input to AC output without an intermediate circuit capacitor. An indirect matrix converter has more advantages and performs better with space vector modulation (SVM) techniques. This article proposed an ANFIS-based SVM technique for the rectifier stage of an Indirect Matrix Converter. The data used to train the ANFIS-based SVM is generated from the traditional SVM. The training methods used for training are the combination of backpropagation and least squares methods. The angle and delay angle are inputs to the proposed scheme and outputs are switching times. Because of this technique; The converter output voltage is improved and THD (Total Harmonic Distortion) of voltage and currents are reduced compared to the traditional SVM. The performance of the converter with ANFIS-based SVM is compared with conventional and the changed SVM by using MATLAB/Simulink.

Keywords: Space vector modulation (SVM), ANFIS (Adaptive Neuro Fuzzy Inference System)-based SVM, Total Harmonic Distortion (THD), Indirect Matrix Converter (IMC), Converter side modulation modified matrix converter, Virtual DC link.

1. Introduction:

The converter that converts from direct AC input power to AC output power is a matrix converter. The matrix converter has various advantages such as: Allowing current flow in both directions, no need for a large intermediate circuit capacitor, the life of the converter is extended due to the lack of a capacitor and it is economical. The matrix converters are grouped such as Direct Matrix converter (DMC) and Indirect Matrix Converter (IMC). The IMC has more advantages than the DMC, such as generating pulses to turn the devices ON (switching) is easy, and turning them OFF (commutating) is also easy. Due to these advantages of an IMC and with bidirectional power flow current source rectifier stage and unidirectional voltage source inverter, it is used in various applications such as electric drives such as controlling an asynchronous motor [1], as an active filter and also in FACT's device for power factor correction and power quality improvement [2.3]. The performance of an IMC depends on the type of modulation scheme used to switch the power electronic devices.

The indirect matrix converter is controlled using a carrier-based modulation method and a space vector method. The carrier based modulation methods are used to control the output voltage with the load of the motor and the slope of the carrier and the voltage offset to get the unity power factor on the input side [4]. Phase Shift and Phase Disposition Carrier based modulation scheme is applied to control the output voltage.

However, the Space Vector Modulation Technics (SVPWM) has better advantages, e.g. B. Simple implementation by using digital controllers like DSP or microprocessor, output current quality, dynamic performance and performance under unbalance conditions are also good [5].

Space vector modulation is applied separately for the rectifier stage and the combination of booster and inverter stages, the rectifier is controlled with the current reference based SVPWM and the inverter is controlled with the voltage reference [6]. In [7] the modulation techniques for IMC are SVPWM and Sinusoidal PWM (SPWM), the rectifier stage is controlled with the SVPWM and an inverter stage is controlled with the SPWM. Carry-based PWM is used to control the IMC, the pulses are generated by comparing the modulation signal with the same triangle for rectifier and inverter, this IMC is used to drive the five-phase motor [8].

The adaptive Sugeno-type neuro-fuzzy controller powered induction motor with current control is presented. This PI technique is replaced by a neuro-fuzzy controller to improve voltage levels and self-tune against speed command fluctuations and load disturbances [9,10]. In order to reduce the common mode voltage by space vector pulse width modulation of matrix converters, the correct selection of the active vectors and the switching sequence is explained [11]. The neuro-fuzzy based SVM powered induction motor is presented. The neuro-fuzzy provides better drive performance with reduced torque ripple compared to neural network and traditional SVM methods [12]. An alternative space vector modulation applied to a matrix converter based induction motor to reduce the common mode voltage. By analysing SVM switching patterns and matrix converter zero vectors replaced by rotating to reduce leakage current and increase motor life [13]. The matrix converter based on space vector modulation offers better performance compared to a traditional matrix converter [14]. The induction motor based on a matrix converter allows better control of torque, flux ripple and low reactive power delivered to the grid at unity power factor [15].

With conventional SVPWM for the rectifier stage, the output is the result of mains input voltages, with this PWM,

*E-mail address: nmurikipudi@gmail.com
ISSN: 1791-2377
doi:10.25103/jestr.155.19

the virtual intermediate circuit shows more fluctuations. However, if the SVPWM for the rectifier stage is changed, the utilization of the DC link increases and the fluctuation of the DC link voltage also decreases. In this work, the modified SVPWM for the rectifier stage is implemented and compared to the ANFIS-based SVPWM for the rectifier stage. The THD of the output current and mains voltages is reduced in ANFIS-based SVPWM.

The paper is structured as follows: Section II explains IMC's modified SVPWM at the rectifier stage and SVPWM for the inverter stage. The implementation of ANFIS-based SVPWM is described in Section III. In section IV, the simulation results are evaluated. Conclusions are presented in Section V.

2. Control of an Indirect Matrix Converter

The schematic diagram of an IMC is shown in Fig 1 and has two conversion levels, one is the rectifier and the other is an inverter levels.

i) Space vector Pulse Width Modulation

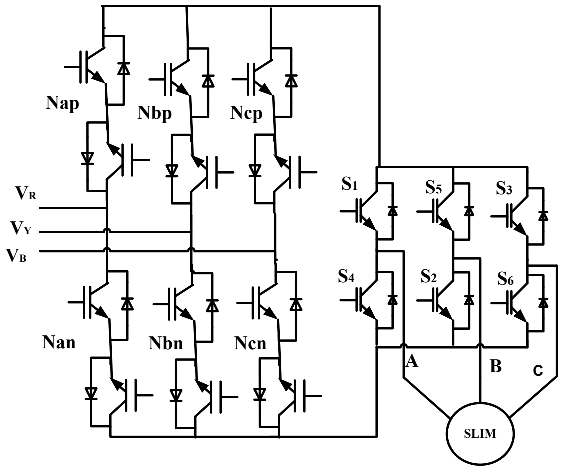

Fig 1. Schematic diagram of IMC

a) Switching of Rectifier Stage

The IMC rectifier stage is a bidirectional power flow current source rectifier and the block diagram is shown in Figure 2.

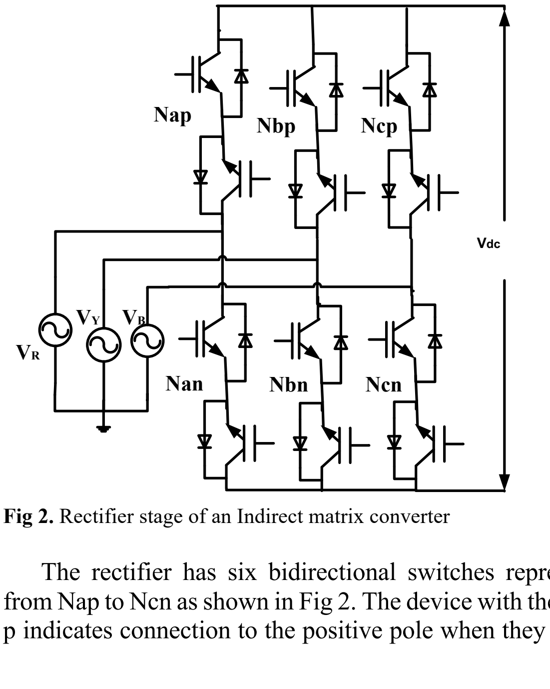

Fig 2. Rectifier stage of an Indirect matrix converter

The rectifier has six bidirectional switches represented from Nap to Ncn as shown in Fig 2. The device with the suffix p indicates connection to the positive pole when they are on, and the suffix n indicates the negative pole when they are on. The suffix a, b and c indicates the connected phase. The three-phase AC input voltages that enter the rectifier are V_R, V_Y, and V_B.

$$
\begin{aligned}
V_R &= V_{\max}\sin\omega t \\
V_Y &= V_{\max}\sin(\omega t - 120^0) \\
V_B &= V_{\max}\sin(\omega t - 240^0)
\end{aligned}
\tag{1}
$$

Where the maximum or peak value of the sinusoidal input voltage is represented by V_{max} and the frequency is represented by ω. The rectifier stage of IMC is controlled by SVM. The hexagon of the space vector is divided into six sectors, the duration of each sector is 60^0 and is shown in Figure 3.

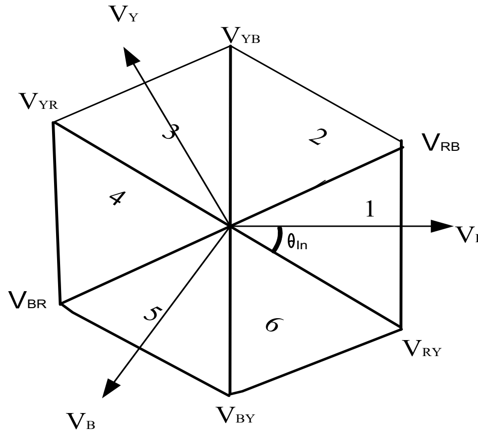

Fig 3. Space vector diagram with different sectors

Process of Space Vector Modulation (SVM):

1. Three phase voltages are converted into two axis – α and β components.
2. Calculate V_{ref} and θ_{in} from V_α and V_β
3. The location of V_{ref} in space vector Hexagon is identified with the help of θ_{in} and the modulation index considered as unity.
4. The Switching times T_p and T_n are calculated and there active vector are responsible to produce the required current in the sector.
5. Switching time of active vectors are calculated using the equations

$$
T_p = T_s \frac{\sin(\frac{\pi}{3} - \theta_{in})}{\sin(\frac{\pi}{3} - \theta_{in}) + \sin\theta_{in}} \tag{2}
$$

$$
T_n = T_s \frac{\sin(\theta_{in})}{\sin(\frac{\pi}{3} - \theta_{in}) + \sin\theta_{in}} \tag{3}
$$

Where T_s is sampling time.

6. Sector and active voltage vector with variation of $\theta_{in} = \omega t$ for modified SVPWM at rectifier stage are shown in Table 1 and the Turn-On Time of each switch in each sector is given Table.2.

Table 1. Active Voltage Vectors of modified SVPWM at rectifier stage

θ_{in}	Sector	DC link voltage
-30 to 30	1	V_{RB}
30 to 90	2	V_{YB}
90 to 150	3	V_{YR}
150 to 210	4	V_{BR}
210 to 270	5	V_{BY}
270 to -30	6	V_{RY}

Table 2. Switching times of modified SVPWM at rectifier stage

Sector	Time of switches					
	A+	A-	B+	B-	C+	C-
1	T_p+T_n	0	0	0	0	T_p+T_n
2	0	0	T_p+T_n	0	0	T_p+T_n
3	0	T_p+T_n	T_p+T_n	0	0	0
4	0	T_p+T_n	0	0	T_p+T_n	0
5	0	0	0	T_p+T_n	T_p+T_n	0
6	T_p+T_n	0	0	T_p+T_n	0	0

b) Switching of Inverter stagey:

At the inverter side also SVM method is used. Space vector hexogen diagram and six active vectors V_1 to V_6 and two Zero vectors V_0 and V_7 are shown Fig 4. The voltage-time balance method is used to determine the switching times T_1 and T_2. In Fig 5, the operational switching times are shown along with active vectors for Sector-1.

$$V_{ref}T_s=V_1T_{1in}+V_2T_{2in}+V_0T_{0in} \tag{4}$$

Where the reference voltage is represented as V_{ref}, the operational switching time of V_1 is T_1, T_2 is the operational time of V_2 and T_0 is the operational time of zero vectors (V_0 &V_7).

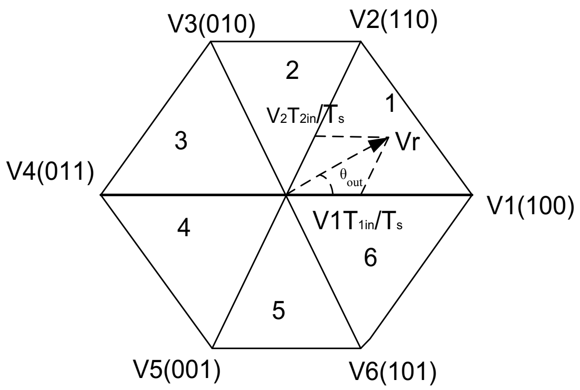

Fig. 4 Space vector Hexogen

The switching times are calculated as

$$T_{1in}=\frac{\sqrt{3}}{V_{dc}}V_rT_s\sin(\frac{\pi}{3}-\theta_{out}) \tag{5}$$

$$T_{2in}=\frac{\sqrt{3}}{V_{dc}}V_rT_s\sin\theta_{out} \tag{6}$$

$$T_{0in}=T_s-T_{1in}-T_{2in} \tag{7}$$

Where the virtual output voltage at the rectifier level is represented as Vdc

The operational switching times of the IMC inverter level are a combination of the switching times of rectifier and conventional inverter operation.

$$T_11=\frac{T_{1in}}{2} \text{ and } T_21=\frac{T_{2in}}{2} \tag{8}$$

The operational switching sequence of IMC inverter level in sector-1 is shown in Fig 5.

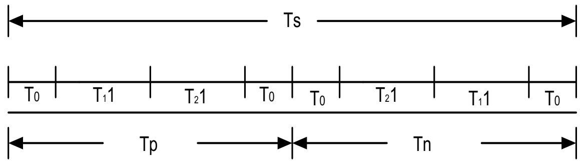

Fig. 5. Switching sequence of IMC inverter level of sector-1

i. ANFIS based SVPWM for rectifier stage:

The ANFIS controller is trained by taking angle α, and α' are input and output are switching timings T_1 &T_2 are outputs. The α, and α' are rectifier input voltage angle and derivative of the an angle respectively.

a) Structure of Adaptive neuro-fuzzy controllers

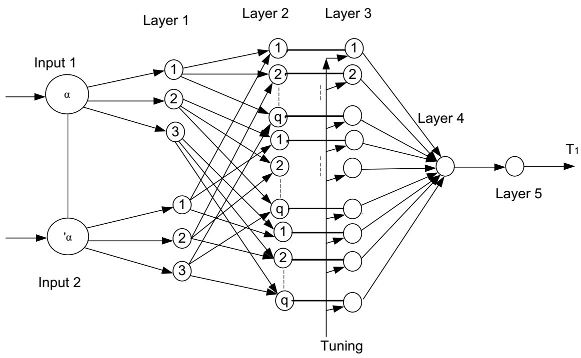

Fig. 6. Structure of five-layer ANFIS for T_1 Switching time

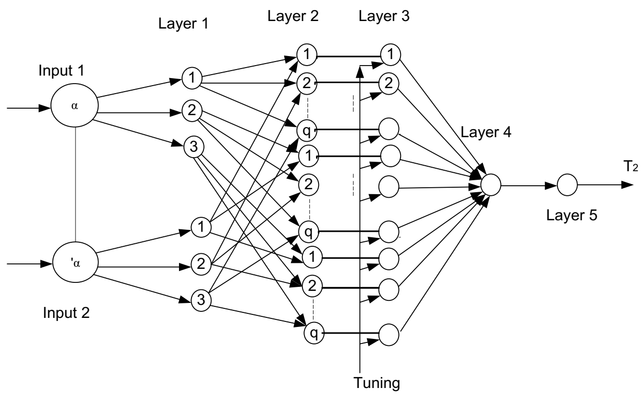

Fig. 7. Structure of five-layer ANFIS for T_2 Switching time

The structure of five-layer ANFIS for switching time T_1 and T2 is shown in fig. 3 and 4.

Layer 1: Let Z'_j be the response of j^{th} node in first layer and input is α_j of j^{th} node of the ANFIS, j = 1, 2, …, q, let a node function N be associated with each node.

$$Z^1 = N_j(\alpha_j) \tag{9}$$

Here, N_1, N_2, …, N_q are the node functions, which are same as the regular fuzzy system membership functions and q is the number of nodes for each input. The Gaussian shieled membership function is used.

Layer 2: The response of each node in layer 2 is the product of all input signals. Each node response represents the trigger strength of a rule.

$$Z_j^2 = N_j(\alpha_j) + N_k(\alpha'_k) \tag{10}$$

Layer 3: The normalized triggering strengths are determining in this Layer.

$$Z_j^3 = \frac{Z_j^2}{\sum_j Z_j^2} \tag{11}$$

Layer 4: It executes Sugeno-type inference system, i.H. the output of each IF-THEN rule is generated from a linear input variables of ANFIS, α_1, α_2,……,α_q and constant term, d_1, d_2, …, d_q. The weighted response sum of an intermediate is the node's response.

$$Z_j^4 = Z_j^3 \sum_{k-1}^{q} Q_k(\alpha'_k) + d_k \tag{12}$$

where Q_1, Q_2, …, Qq and d_1, d_2, …, d_q, are consequent parameters in this layer.

Layer 5: This layer response is similar to the defuzzification processor of a fuzzy system using weighted average method. It generates the output by summing its input signals.

$$Z_j^5 = \sum_j Z_j^4 \tag{13}$$

This output Z_j^5 is the T_1 for this example.

b) Learning algorithm

The ANFIS controller is initially taken as a fuzzy model and tuned using a backpropagation least squares combinatorial algorithm. In each epoch the difference between an actual response and a required response is measured, it is an error. The error size is reduced. The training process ends when either the error rate or the specified number of epochs is reached.

3. Results and Discursion

Simulation results

When the changes of SVPWM for rectifier stage is changed the virtual DC voltage magnitude variations are reduced and distortion in DC voltage is reduce. Fig. 8 shows the DC virtual link voltage with the conventional SVPWM. The magnitude is varied from 400 V to 740 V and have distortions. Fig.9 and 10 show the DC virtual link voltage waveform of changed SVPWM for rectifier stage and ANFIS SVPWM for rectifier stage respectively. The voltage magnitude is varied from 640V to 740V and waveform is smooth.

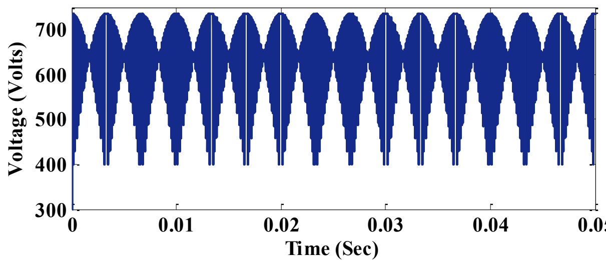

Fig. 8. Virtual DC link voltage waveform with conventional SVPWM

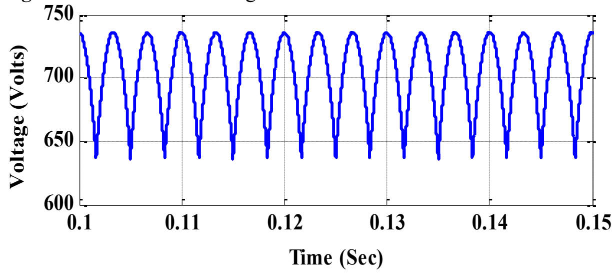

Fig. 9. Virtual DC link voltage with modified SVPWM at rectifier stage

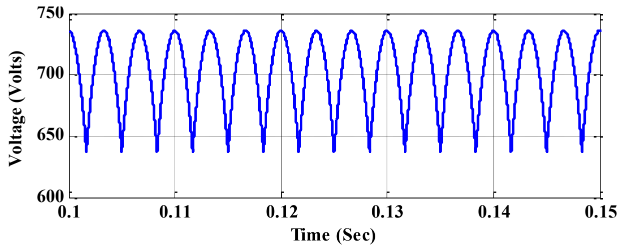

Fig. 10. Virtual DC link voltage waveform with ANFIS SVPWM

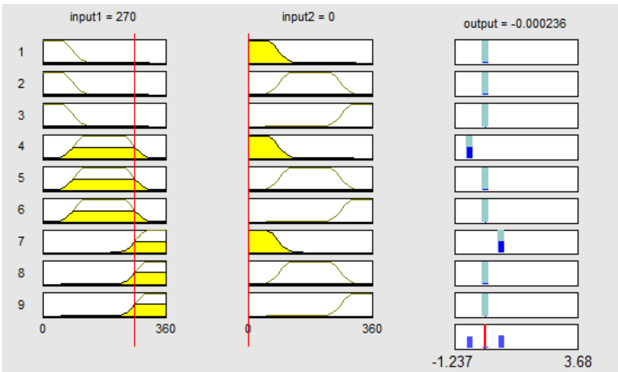

Fig. 11. Fuzzy rules of Switching time T_1

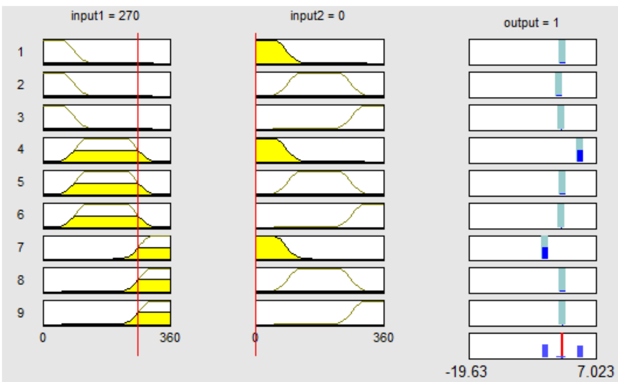

Fig. 12. Fuzzy rules of Switching time T_2

Fig. 11 and 12 show the funny rules of switching times T_1 &T_2 in ANFIS SVPWM.

Fig. 13, 14 and 15 show the supply current waveforms in conventional, changed and ANFIS based SVPWM respectively, the magnitude is varied from 30 A to -30 A peak to peak. The supply side current waveform has more distortion when it is operated with conventional SVPWM than the changed and ANFIS based SVPWM.

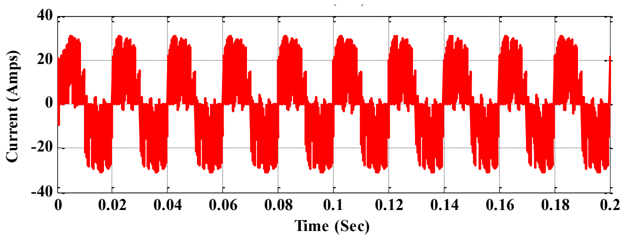

Fig. 13. Supply side current waveform with conventional SVPWM

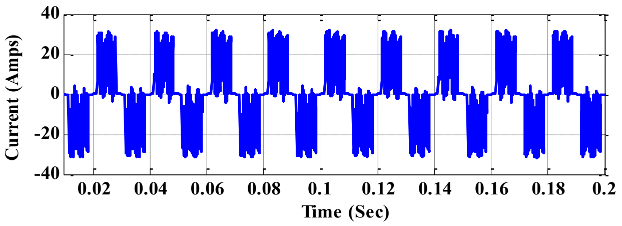

Fig. 14. Supply side current waveform with modified SVPWM at rectifier stage.

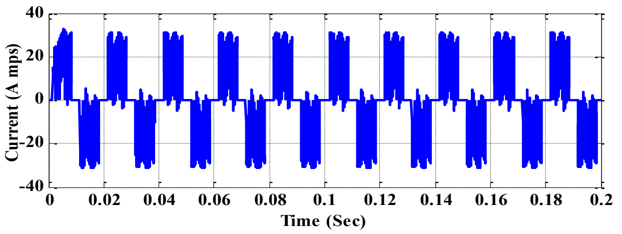

Fig. 15. Supply side current waveform with ANFIS SVPWM

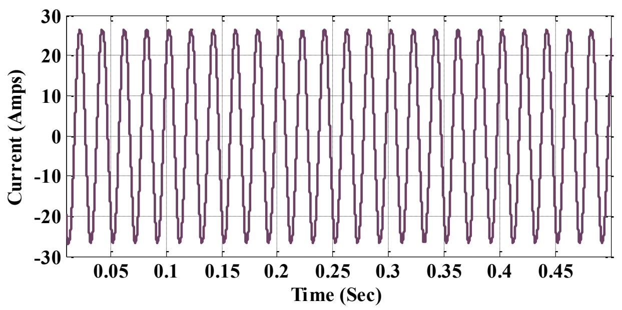

Fig. 16. Load current waveform with conventional SVPWM

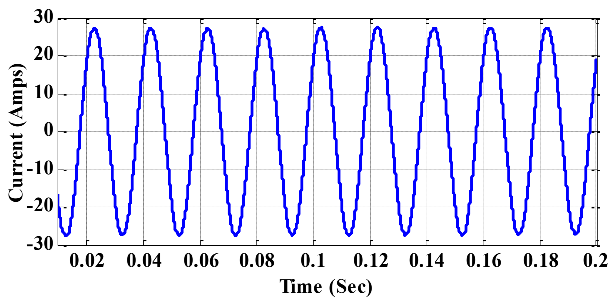

Fig. 17. Load current waveform with modified SVPWM at rectifier stage

Fig. 16,17 and 18 show the load current with conventional, Changed and ANFIS based SVPWM respectively. The current magnitude is varied from +29 A to -29 A and the current waveform has distortion what is controlled with conventional SVPWM. The line output voltage waveforms at conventional, Changed and ANFIS based SVPWM are shown in Fig. 19,20 and 21 respectively.

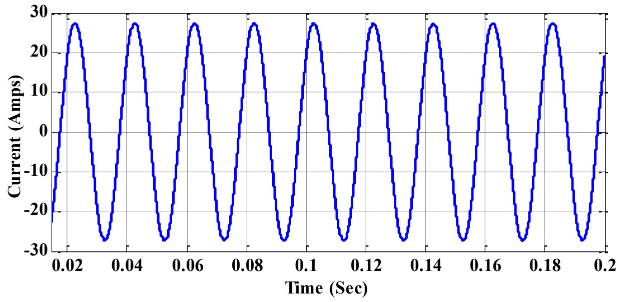

Fig. 18. Load current waveform with ANFIS SVPWM.

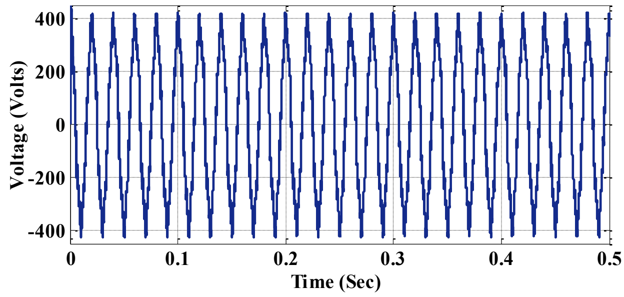

Fig. 19. Output load voltage with conventional SVPWM

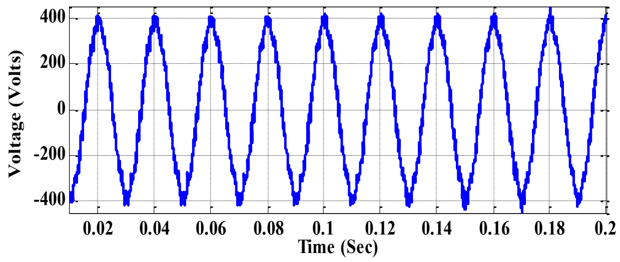

Fig. 20. Output load voltage with modified SVPWM at rectifier stage

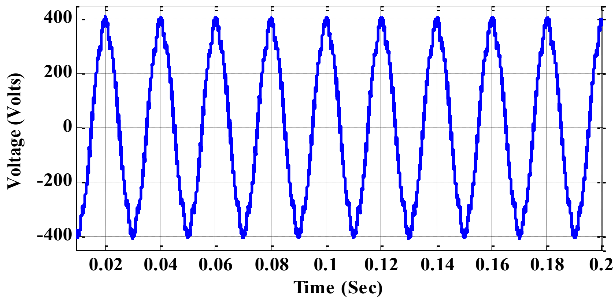

Fig. 21. Output load voltage wave form with ANFIS SVPWM

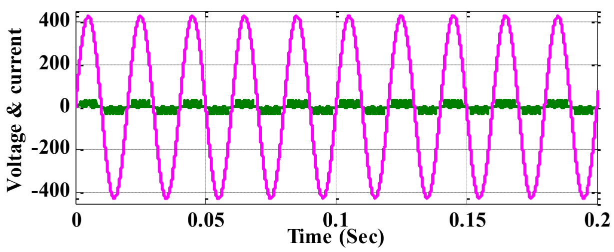

Fig. 22. Supply side single phase voltage and current waveforms with conventional SVPWM

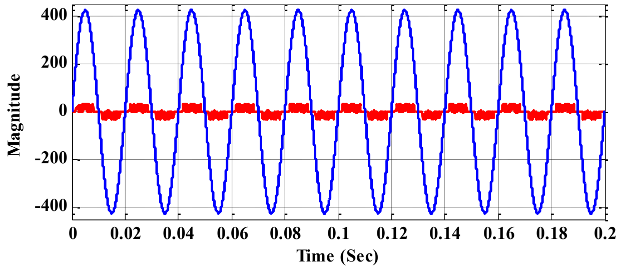

Fig. 23. Supply side single phase voltage and current waveforms with modified SVPWM at rectifier stage

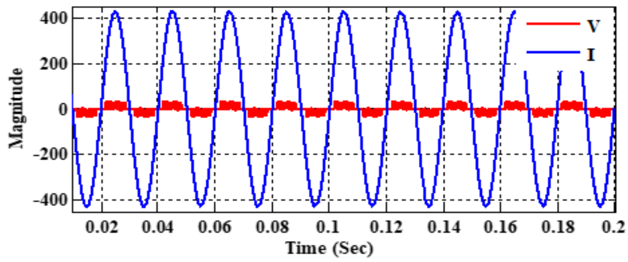

Fig. 24. Supply side single phase voltage and current waveforms with ANFIS SVPWM.

Figures 22, 23 and 24 show the supply side single phase voltage and current waveforms with conventional, modified and ANFIS based SVPWM. The phase angle between voltage and current waveforms is zero. Therefore, a unity power factor is maintained on the input side of the IMC, even the power factor on the load side is not unity. The voltage across the R-phase load and its current waveforms at different SVPWM are show in Fig. 25,26 and 27. The phase angle difference between the load voltage and current is 43.30, and p.f is 0.73.

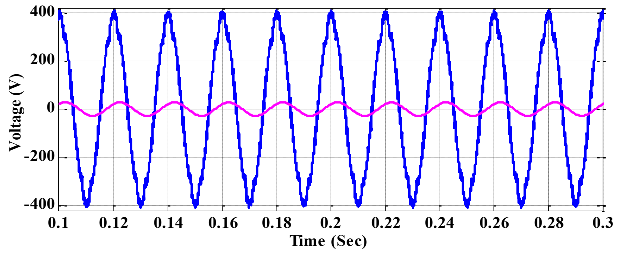

Fig. 25. Voltage across the R-phase load and its current waveforms with conventional SVPWM.

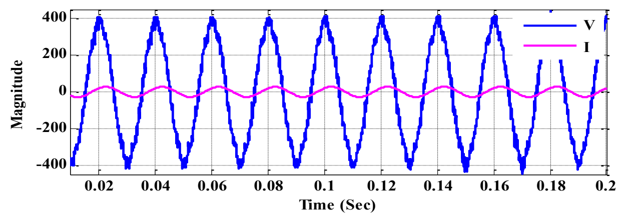

Fig. 26 Voltage across the R-phase load and its current waveforms with modified SVPWM at rectifier stage.

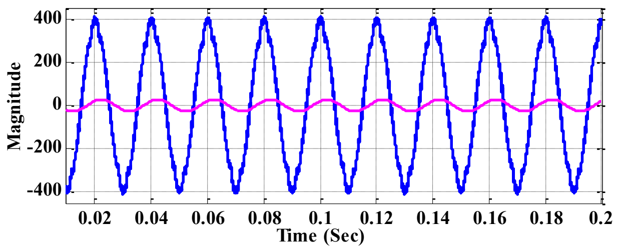

Fig. 27 Voltage across the R-phase load and its current waveforms with ANFIS SVPWM.

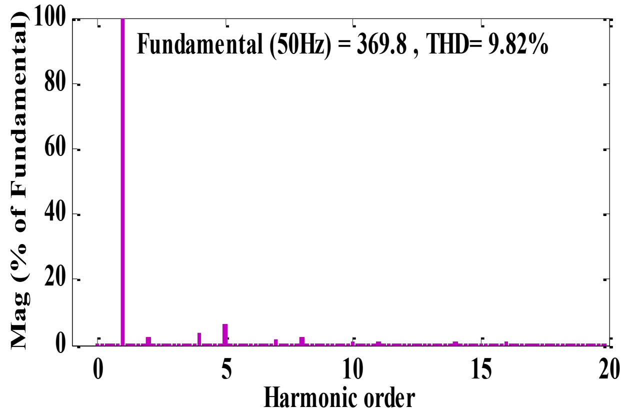

Fig. 28. Output phase voltage THD conventional SVPWM

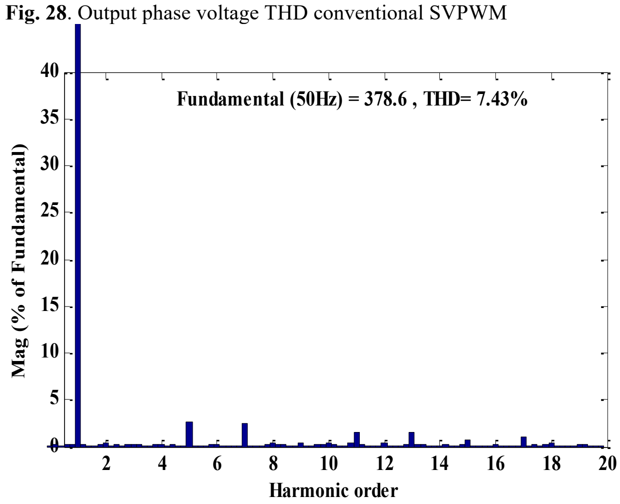

Fig. 29. Output phase voltage THD with modified SVPWM at rectifier stage

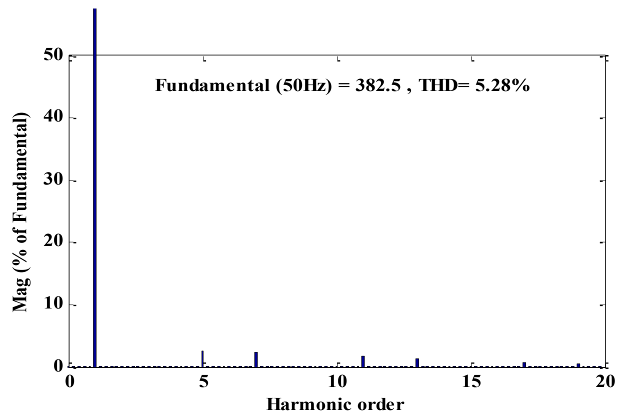

Fig. 30. Output phase voltage THD with ANFIS SVPWM

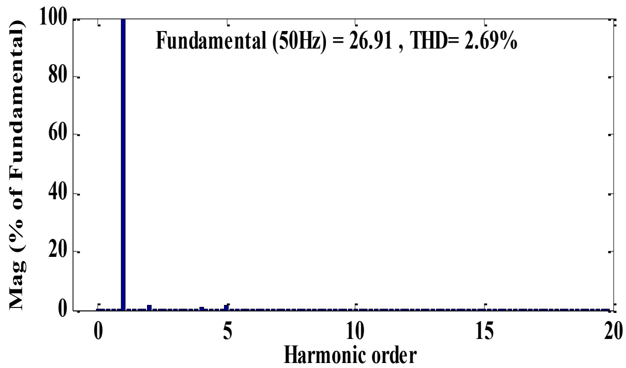

Fig. 31. Output current THD conventional SVPWM

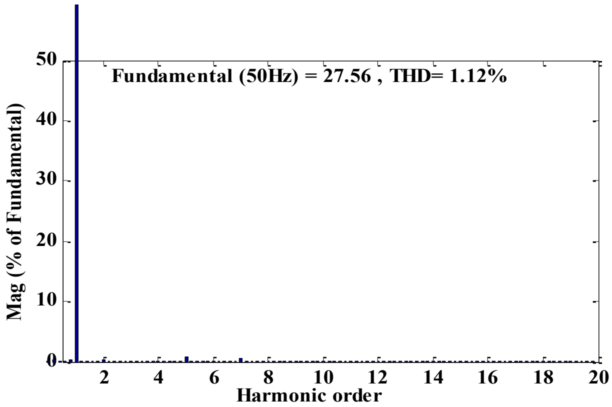

Fig. 32. Output current THD with modified SVPWM at rectifier stage

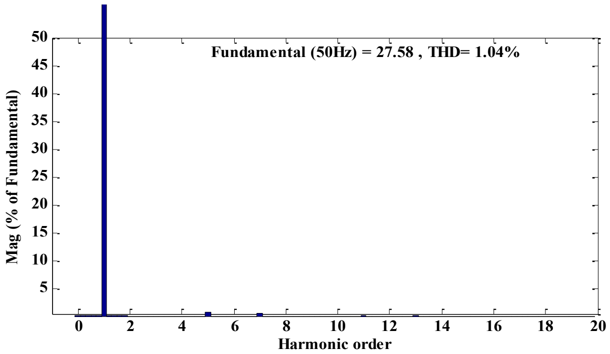

Fig. 33. Current THD with ANFIS SVPWM

The THD of load line voltage and current with conventional, modified and ANFIS based SVPWM are show is Fig.28 to Fig.33. The load phase voltage THD is reduces from 9.82% to 5.28% and fundamental component is improved from 369.8 V to 382.5 V, when compared with compared with the conventional and ANFIS based SVPWM. The percentage change in reduction of THD is 48.9% and improvement fundamental component is 3.43%. The reduction of current THD is from 2.69% to 1.04% and improvement in fundamental component is 26.91 to 27.58.

Table 3 comparison of Voltage and current THD & Fundamental components

S.No	Type of SVPWM	Current THD	Fundamental Component of voltage	Fundamental Component of current
1	Conventional	2.69	369.8	26.91
2	Modified SVPWM at Rectifier side	1.12	378.6	27.56
3	ANFIS based	1.04	382.5	27.58

4. Conclusion

In this paper, the performance of an indirect matrix converter with conventional, changed and ANFIS based SVPWM for rectifier stage are analysed by considering the phase load voltage and load currents. The parameters which are considered for analysis are THD and fundamental component when an indirect matrix converter is fed to R-L load. From the results, observed that ANFIS based SVPWM for rectifier stage produce better performance than remaining conventional and changed SVPWM. The THD of the voltage & currents are reduced by 48.9% and 61.3% and the fundamental component of voltage & current are improved by 3.43% and 2.48% respectively.

References

1. J. Riedemann, J. C. Clare, P. W. Wheeler, R. Blasco-Gimenez, M. Rivera and R. Peña, "Open-End Winding Induction Machine Fed by a Dual-Output Indirect Matrix Converter," in *IEEE Transactions on Industrial Electronics*, vol. 63, no. 7, pp. 4118-4128, July 2016, doi: 10.1109/TIE.2016.2531020.
2. Y. Sun, X. Li, M. Su, H. Wang, H. Dan and W. Xiong, "Indirect Matrix Converter-Based Topology and Modulation Schemes for Enhancing Input Reactive Power Capability," in *IEEE Transactions on Power Electronics*, vol. 30, no. 9, pp. 4669-4681, Sept. 2015, doi: 10.1109/TPEL.2014.2363656.
3. L. Empringham, J. W. Kolar, J. Rodriguez, P. W. Wheeler and J. C. Clare, "Technological Issues and Industrial Application of Matrix Converters: A Review," in *IEEE Transactions on Industrial Electronics*, vol. 60, no. 10, pp. 4260-4271, Oct. 2013, doi: 10.1109/TIE.2012.2216231.
4. Y. Sun, W. Xiong, M. Su, X. Li, H. Dan and J. Yang, "Carrier-Based Modulation Strategies for Multimodular Matrix Converters," in *IEEE Transactions on Industrial Electronics*, vol. 63, no. 3, pp. 1350-1361, March 2016, doi: 10.1109/TIE.2015.2494871.
5. H. S. Purnama, T. Sutikno and M. Facta, "Modulation Strategies for Indirect Matrix Converter: Complexity, Quality and Performance," *2018 5th International Conference on Electrical Engineering, Computer Science and Informatics (EECSI)*, 2018, pp. 97-100, doi: 10.1109/EECSI.2018.8752702.
6. M. Raghuram, A. K. Chauhan and S. K. Singh, "High-Gain-Integrated Switched Capacitor Indirect Matrix Converter," in *IEEE Journal of Emerging and Selected Topics in Power Electronics*, vol. 7, no. 3, pp. 1846-1853, Sept. 2019, doi: 10.1109/JESTPE.2018.2863551.
7. A. Ammar, H. Y. Kanaan, N. Moubayed, M. Hamouda and K. Al-Haddad, "Original Approach Toward Three-Phase Indirect Matrix Converters Through Hybrid PWM Modulation and DSP Implementation," in *IEEE Access*, vol. 8, pp. 45837-45852, 2020, doi: 10.1109/ACCESS.2020.2977502.
8. T. D. Nguyen and H. -H. Lee, "Development of a Three-to-Five-Phase Indirect Matrix Converter With Carrier-Based PWM Based on Space-Vector Modulation Analysis," in *IEEE Transactions on Industrial Electronics*, vol. 63, no. 1, pp. 13-24, Jan. 2016, doi: 10.1109/TIE.2015.2472359.
9. Meliani Bouziane and Meroufel Abdelkader, " Direct space vector modulation for matrix converter fed dual star induction machine and neuro-fuzzy speed controller", Bulletin of Electrical Engineering and Informatics, Vol. 8, No. 3, pp.818-828, 2019.
10. Khaliqur Rahman, Nasser Al-Emadi, Mohammad Al-Hitmi, Atif Iqba, "CMV reduction in a three-to-seven phase direct matrix converter using SVPWM", IET Electric Power Applications, Vol. 13, no. 8, pp. 1219-1228, 2019.
11. Durga Sukumar, Jayachandranath Jithendranath & Suman Saranu, "Three-level Inverter-fed Induction Motor Drive Performance Improvement with Neuro-fuzzy Space Vector Modulation", Electric Power Components and Systems, vol.42, pp.1633–1646, 2014
12. Jordi Espina, Carlos Ortega, Liliana de Lillo and Lee Empringham, "Reduction of Output Common Mode Voltage Using a Novel SVM Implementation in Matrix Converters for Improved Motor Lifetime", IEEE Transactions on Industrial Electronics, Vol. 61, No. 11, pp. 5903-5911, 2014.
13. Meng Yeong Lee, Patrick Wheeler, and Christian Klumpner, "Space-Vector Modulated Multilevel Matrix Converter", IEEE Transactions on Industrial Electronics, Vol. 57, No. 10, pp.3385-3394, 2010.
14. Ren´e Vargas, Ulrich Ammann and Jose Rodriguez, "Predictive Torque Control of an Induction Machine Fed by a Matrix Converter

With Reactive Input Power Control", IEEE Transactions on Power Electronics, Vol. 25, No. 6, pp.1426-1438, 2010.
15. Hong-Hee Lee and Hoang M. Nguyen, "An Effective Direct-SVM Method for Matrix Converters Operating With Low-Voltage Transfer Ratio", IEEE Transactions on Power Electronics, Vol. 28, No. 2, pp.920-929, 2013.

Appendix:

Indirect matrix converter:
Input supply: 3 Phase, 520 V, 50Hz.
Output: 3 Phase, 490 V, 50 Hz.
IGBT: Ideal IGBT with R_{in}=1 Milli Ohms, R_s=0.1M Ohms and C_s=Inf
Load: R=10 Ohms, L=30 mh
Filter: R_f=100 Ohms, L_f=2 mh and C_f=2 μF